

Holistic Lignin Valorization *via* Flow Photocatalysis towards vanillin and bioplasticizers

Xavier Marset,^[a] Salvador Montilla-Verdú,^[a] Elio Rico,^[a] Jaume Gómez-Caturla,^[b] Mario Miranda-Pinzón,^[b] Rafael Balart,^{,[b]} Ulrich Aschauer,^{*,[c]} Néstor Guijarro^{*,[a]}*

^[a] Institute of Electrochemistry, Universidad de Alicante, Apdo. 99, 03080 Alicante, Spain.

^[b] Instituto Universitario de Investigación de Tecnología de Materiales (IUITM), Universitat Politècnica de València (UPV), Plaza Ferrándiz y Carbonell 1, 03801, Alcoy, Spain.

^[c] Department of Chemistry and Physics of Materials, University of Salzburg, 5020, Salzburg, Austria

Abstract

Lignin valorization has become an urgent priority due to its status as the most abundant natural biopolymer containing aromatic structures, yet industrially unexploited. In this study, we present a photocatalytic method using a simple anthraquinone catalyst to break down lignin's recalcitrant structure into valuable monomers. Notably, this process is described under flow conditions for the first time. The monomer yields achieved are the highest reported in literature, although lignin is not fully depolymerized. However, the remaining oligomers can be effectively repurposed as polylactic acid (PLA) plasticizers, significantly enhancing PLA's mechanical properties and imparting shape-memory behavior. Thus, by processing lignin through a photochemical flow reactor, it is fully converted either into industrially relevant monomers, such as vanillin and syringaldehyde, or fragmented sufficiently for use as PLA plasticizers. This approach ensures that no wasteful by-products are generated, offering a sustainable pathway for lignin valorization.

Introduction

For the past two decades, society has been repeatedly warned about the imminent depletion of fossil fuel reserves, yet for the vast majority of people this fact impacted solely on the decision on whether it is the right time to purchase an electric vehicle. However, the dire consequence of this reliance on petrochemical industry is not only the continuous rise in costs¹ but also the escalating environmental damage due to greenhouse gas emissions. To address this, the 2015 Paris Agreement introduced limits on oil extraction.^{2, 3} However, the significance of petrochemicals extends far beyond fuels. They are the foundation of many essential products in our modern lives, from polymeric materials to pharmaceuticals, all of which rely on key components derived from petroleum.⁴ As a result, the need to seek alternative energy solutions has become urgent, but equally critical is the development of renewable sources for chemical feedstocks.^{5, 6}

Today, lignocellulosic biomass is considered a valuable resource, though its potential remains largely untapped due to the lack of efficient valorization

technologies.⁷ This type of biomass consists of cellulose, hemicellulose, and lignin. Both cellulose and hemicellulose have found various applications, such as in the paper industry or ethanol production for cellulose,^{8,9} and in the production of materials and fine chemicals like xylitol and furfural for hemicellulose.¹⁰ However, lignin, which makes up approximately 25% of the total wood mass, is still regarded as a waste product. Despite being the primary by-product of the pulp and paper industry, less than 3% of lignin is used to produce commercial compounds, with the rest being burned as low-energy fuel.¹¹

This fact is better understood when examining Lignin's chemical structure. Lignin is a biopolymer formed by aromatic monomers in a sequence and structure which are not well-defined. Its biosynthesis is performed on cell walls in an irregular manner *via* free-radical coupling mechanisms, resulting in an extremely complex structure.¹² There are primarily three main repeating units (monolignols), arranged in random sequences. The major contributors to lignin's primary structure are *p*-coumaryl (H), coniferyl (G), and sinapyl (S) alcohols, making lignin an unrivaled source for obtaining aromatic compounds without depending on petroleum.¹³ But despite having only three main monomers, the lignification process occurring in plants produces a recalcitrant material from which obtaining usable monomers is not a trivial matter.

Over the last decades, several methodologies to valorize lignin have been proposed,¹⁴ including pyrolysis,¹⁵ hydrogenolysis,¹⁶ acid/base depolymerization¹⁷ or oxidation.¹⁸ However, up to now most of these methods are (i) energy-intensive, which increases costs and environmental impact, and depends on (ii) harsh treatments that irreversibly alter the nature of the aromatic compounds, thereby reducing the profit margin in the market. Recently, the use of photocatalytic systems has been proposed to carry out lignin fragmentation. These systems allow for more selective fragmentation, operating under ambient conditions and using only solar energy to activate the process. Some of the recent examples of photocatalytic lignin valorization make use of metallic species, like vanadium¹⁹ tungsten²⁰ or iridium²¹ complexes (figure 1). Despite the versatility of some of these catalysts, several disadvantages limit their applicability, including the typically high price and the inconvenient heavy metal contamination of products if drug or alimentary products are intended to be produced. In addition, these types of processes are performed under batch conditions, being not suitable for large-scale applications due to some disadvantages for scaling up; mainly (i) the reactor must be completely stopped after each reaction to extract the system's contents and isolate the reaction products, and (ii) additional processes are necessary to recover the catalyst after each reaction. Furthermore, most of these processes have been limited to lignin model compounds or have focused on qualitative lignin fragmentation without achieving actual monomer isolation. Consequently, a continuous flow method for producing valuable aromatic aldehydes from lignin remains absent from the literature.

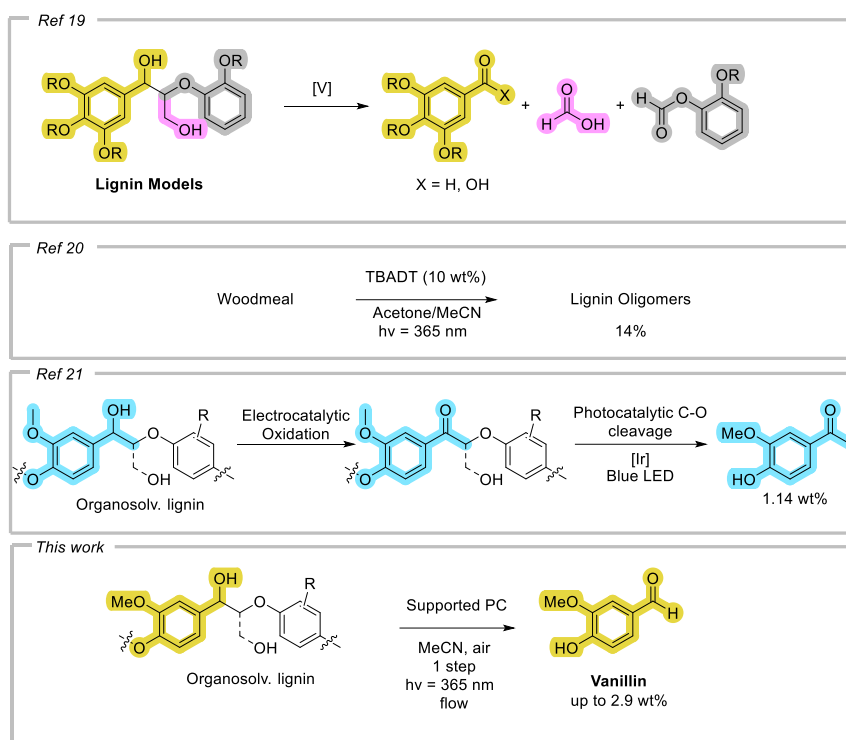


Figure 1. Literature reports of photocatalytic lignin depolymerization.

Results and discussion

Thus, we envisioned the development of a photocatalytic lignin valorization process, but seeking a potential industrial applicability, metallic catalysts were avoided and the use of an inexpensive organic photocatalyst was envisioned. More specifically, we focused our attention on anthraquinones, which are a group of natural pigments found in common dyes that have been proposed as versatile and inexpensive photosensitizers.^{22, 23} These compounds possess high absorptivity and are effective hydrogen atom acceptors, being able to oxidize molecules under photocatalytic conditions using atmospheric O_2 as terminal oxidant.²²

To start with this endeavor, the photochemical cleavage of 2-phenoxy-1-phenylethanol (**2a**) was chosen as model reaction, as it serves as a proof of concept of the system ability to break the β -O-4 bonds present in lignin structure. A survey of reaction conditions was performed, including different solvents,²⁴ photocatalysts and additives. The highest conversion was obtained using 20 mol% of anthraquinone in MeCN, while other solvents like DCM or HFIP afforded good conversion of **2a** but low selectivity towards the β -O-4-like bond cleavage, yielding oxidized byproducts like 2-phenoxy-1-phenylethan-1-one, among others. It is worth noting that performing the reaction under air atmosphere boosted the conversion, although slightly varying the product selectivity (table 1, entries 1-2). It was observed that along with benzaldehyde (**3a**), benzoic acid (**3a'**) was also obtained as an oxidation product of the former when the reaction was performed under extended reaction times, although carefully controlling the reaction time could maximize the ratio of products **3a/3a'**. In addition, instead of finding phenol (**4a**) and anisole (**4a''**) as a result of the bond cleavage, phenyl

formate (**4a'**) was obtained as a major product. To gain some insight on the reaction mechanism, we performed some control experiments. When a solution of **2a** was irradiated for 16 h without catalyst the starting material was recovered almost entirely, proving the role of anthraquinone as photocatalyst (Table 1, entry 3). Since a radical mechanism is expected, a reaction was set under standard conditions but adding 2 equivalents of TEMPO as a radical scavenger. The reaction was greatly inhibited, observing only 4% conversion to benzaldehyde. In addition, we were able to isolate one adduct of TEMPO with a fragment of PPol, providing some insights on the mechanistic pathway of the reaction (table 1, entry 4, figure 2A).

Table 1. Control experiments.

$ \begin{array}{c} \text{MeCN (0.1 M)} \\ \text{AQ (20 mol\%)} \\ \xrightarrow[16\text{ h}]{365\text{ nm}} \\ \text{Ph-CH(OH)-OPh} \quad \text{2a} \quad \rightarrow \quad \text{Ph-CHO} \quad \text{3a} + \text{Ph-COOH} \quad \text{3a'} + \text{PhOH} \quad \text{4a} + \text{PhO-COOH} \quad \text{4a'} + \text{PhOMe} \quad \text{4a''} \end{array} $								
Entry	Variation of stnd cond.	Conv. (%)	PhCHO	PhCO ₂ H	PhOH	PhCOOH	PhOMe	
1	Argon	58	41%	-	14%	-	13%	
2	Air	99	63%	14%	14%	42%		
3	No catalyst	2	1	1	-			
4	TEMPO	5	4	-	-	-	-	

Reaction conditions: To a vial containing **2a** (21.4 mg, 0.1 mmol) and anthraquinone (4.1 mg, 0.02 mmol), MeCN (1 mL) was added. The reaction mixture was stirred at room temperature under irradiation using a 365 nm LED lamp for 16 h.

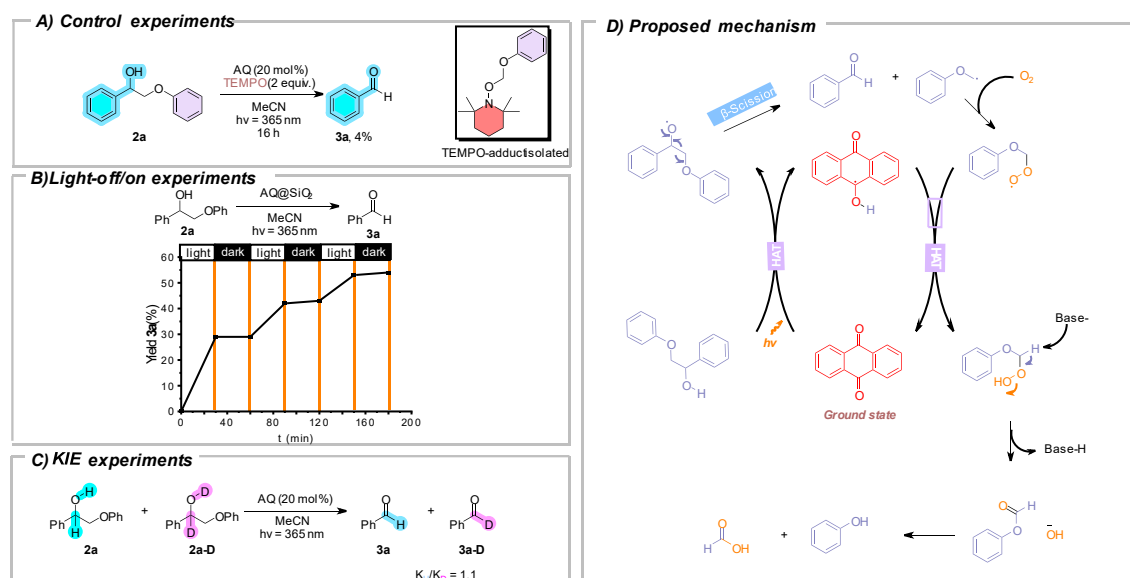


Figure 2. Mechanistic tests: a) Reaction performed with TEMPO as radical scavenger. B) Light on/off experiment. C) Kinetic isotopic effect experiment. D) proposed reaction mechanism.

Moreover, light/dark experiments were conducted, corroborating that the reaction does not proceed without irradiation, which excludes a radical-chain type

process (figure 2B).²⁵ Deuteration experiments were also conducted to shed some light on the reaction mechanism. The deuterated substrate **2a-D** was synthesized and tested in the model reaction. When it was employed as substrate, deuterated benzaldehyde was obtained (**3a-D**), while using it in competition in an equimolar amount of **2a** for short reaction times afforded a product ratio of **3a_H**/**3a_D** = 1.1, indicating that the hydrogen atom transfer (HAT) process is probably not a turnover limiting step for this reaction.²⁶

Based on these results, a possible reaction mechanism was proposed (Figure 2D). Similar reported reaction pathways start with a C_β-H dehydrogenation process, leading C_α-C_β cleavage.²⁷ In contrast, the present reaction might begin with compound **2a** undergoing a hydrogen atom transfer process facilitated by the excited anthraquinone. This step triggers a radical rearrangement, resulting in the release of benzaldehyde (**3a**) and a radical anisole intermediate. The intermediate, whose presence was proven by trapping it with TEMPO, confirms this pathway (Figure 2A). Anisole radical can then follow two mechanisms: it may either extract another hydrogen atom from the substrate or react with molecular oxygen to form an oxidized intermediate. This intermediate undergoes a second HAT event, regenerating the catalyst and releasing phenyl formate (**4a'**). Subsequently, phenyl formate can degrade in the presence of water into phenol (**4a**) and formic acid (detected by ¹H NMR, see Figure S2).

These findings are in stark contrast with most photocatalyzed lignin fragmentation processes, in which the bond cleavage is produced at the C_β-O ether bond, affording acetophenone instead of benzaldehyde.^{20, 21} In some reports, the process starts with HAT removing the hydrogen atom directly attached to C_α or by removing one electron from the aromatic ring,²⁸ but we proposed an O-H bond cleavage to start the catalytic cycle. To gain more insight into which mechanism is more probable using anthraquinone as catalyst, DFT calculations were performed, and the two different approaches were compared in energy. As can be seen in figure 3, the C-H dehydrogenation approach is *c.a.* 50 kcal/mol more energetic than the O-H pathway.

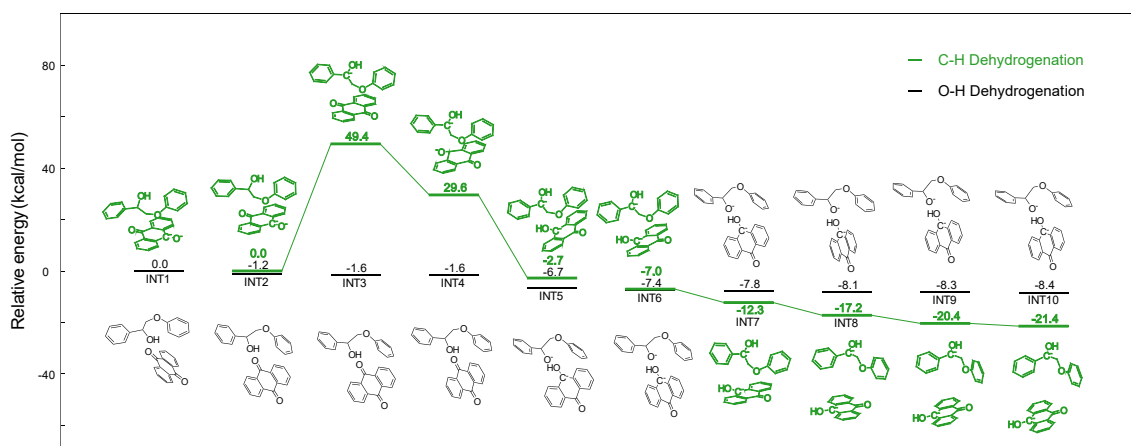


Figure 3. Reaction profiles computed with the NWChem 7.0.2 package²⁹ at the B3LYP/6-31G** level of theory^{30, 31, 32, 33} for the C-H (green) and O-H (black) dehydrogenation pathways of PPOl with anthraquinone.

Once anthraquinone was demonstrated to be an efficient photocatalyst for β -O-4 bond cleavage in a simple lignin model compound (**2a**) under homogeneous conditions, we decided to go one step further to improve the applicability of the method and envisioned a supported catalytic system to adapt this approach to a heterogeneous catalysis. Such a transition would make the method more suitable for industrial upscaling, as the catalyst could be easily recovered after the reaction and used in a continuous-flow photocatalytic reactor. Even though anthraquinone is an organic and inexpensive molecule, performing the lignin valorization in the presence of this catalyst in a homogeneous way would mean an extra purification step. In addition, the presence of these catalysts in the crude product could be potentially problematic for applications on the cosmetic, alimentary, or pharmaceutical industries.³⁴ However, using a supported photocatalyst in which units are immobilized on a fixed bed,³⁵ those problems would be solved. To do so, several inexpensive supports were chosen, including polystyrene-based resins,³⁶ glass wool,³⁷ silica gel³⁸ and alumina³⁹ (see supporting information page S4), with best results obtained with silica-supported anthraquinone (AQ@SiO₂)

With an efficient heterogeneous system developed, catalyst recyclability was studied. Thus, the model reaction was performed in the presence of AQ@SiO₂. Once the reaction was completed, the catalyst was recovered by centrifugation, dried *in vacuo* and reused for a new cycle with a fresh solution of **2a**. In this way, the catalyst was used for 5 cycles without a detrimental effect on the reaction yield or selectivity (Figure 4B). Being proved that the heterogeneous photocatalyst could perform the model reaction, a photocatalytic flow reactor was built. To do so, a peristaltic pump was used to make the starting material solution pass through a transparent column (1 cm internal diameter) inert to the employed radiation. This column was filled with the supported catalyst, ensuring that the reaction takes place as the solution flows through the column (Figure 4C). Reaction profiles were plotted, observing that the reaction is even faster using the supported catalyst (either on batch or under flow conditions, Figure 4A) than using unsupported anthraquinone. It is expected that using longer and thinner columns can greatly improve the reaction rate and efficiency in potential industrial application.⁴⁰

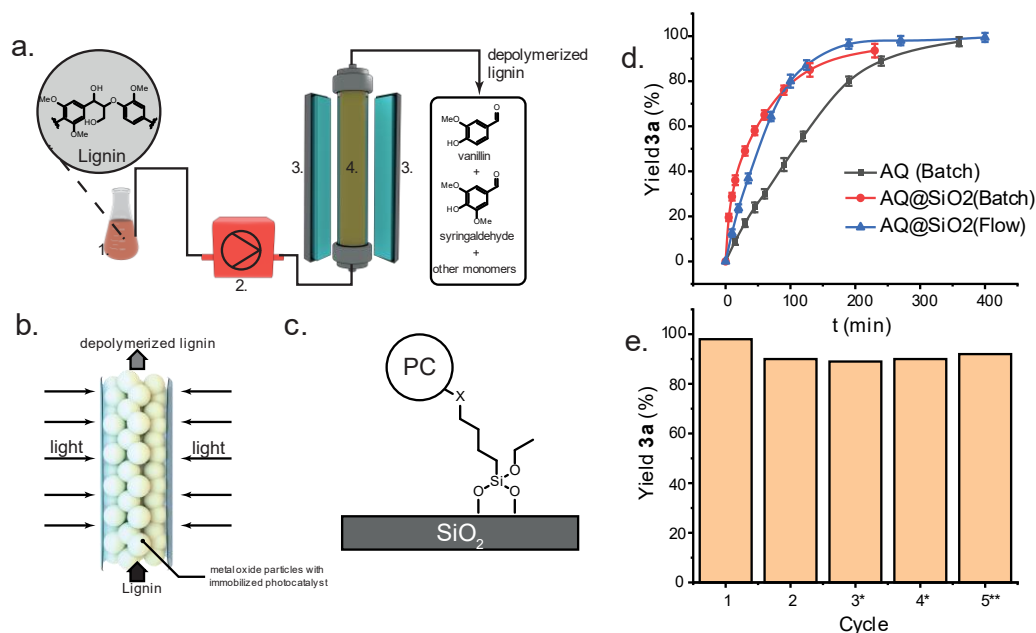


Figure 4. a) Schematic representation of photochemical flow reactor. b) Schematic representation of the transparent column filled with supported catalyst. c) Schematic representation of supported catalyst on silica particles. d) Reaction profile of **2a** cleavage with different catalytic systems, e) Recyclability study of the catalyst for cleavage of **2b** using AQ@SiO₂ reaction time 4 h. * indicates a reaction time of 10 h, ** indicates a reaction time of 16 h.

With the development of three equivalent catalytic systems— i) anthraquinone (AQ), ii) silica-supported anthraquinone under batch conditions (AQ@SiO₂ batch), and iii) silica-supported anthraquinone under flow conditions (AQ@SiO₂ flow)—a study was conducted using increasingly complex lignin model dimers. Initially, dimer **2a** was substituted with other dimers featuring various functional groups that mimic structures found in native lignin (Figure 5). As outlined in the reaction mechanism, the photocatalyzed cleavage of **2a** predominantly yields benzaldehyde, which can be further oxidized to benzoic acid under prolonged exposure to air. This C–C bond cleavage also generates an anisole radical that can evolve into several products, primarily anisole, phenyl formate, or phenol. However, this radical may also form other by-products. The resulting phenolic compounds, such as phenol or guaiacol, are unstable under the reaction conditions, which accounts for their lower yields compared to the carbonylic compounds. When compound **2b**, containing a methoxy group on the phenolic ring, was used as a substrate, the selectivity shifted due to the compound's electronic properties. The C–C cleavage was incomplete, yielding α -hydroxyacetophenone in addition to benzaldehyde. Although **2b** is not representative of the most common structures in native lignin, it provides insight into how substrate nature influences reactivity. Given the intrinsic complexity of natural lignin, a mixture of products is typically expected. Compound **2c**, incorporating an additional carbon (Cy) found in real lignin, was tested to assess its impact on reactivity. The cleavage proceeded similarly, releasing a formic acid molecule without significant changes in the reaction pathway (Figure S2). Introducing an extra methoxy group on the benzylic ring (compound **2d**) afforded similar

reactivity to the one observed with **2a**, yielding primarily *p*-methoxybenzoic acid when using anthraquinone or silica-supported anthraquinone as catalysts. As previously noted, the aldehydes formed can be oxidized to carboxylic acids in the presence of air. Interestingly, conducting the reaction with **2d** under flow conditions inhibited acid formation, selectively producing the aldehyde due to reduced oxygen availability in the packed column. Finally, compounds **2e** and **2f** were successfully cleaved under all three catalytic conditions. However, **2f** exhibited slower reaction rates in batch systems, achieving full conversion in 16 hours under flow conditions.

$\text{Ar}^1\text{CH}(\text{OH})\text{CH}(\text{OR}^1)\text{OAr}^2 \xrightarrow[\text{MeCN, 365 nm, 16 h, air}]{\begin{matrix} \text{AQ (batch)} \\ \text{AQ@SiO}_2 \text{ (batch)} \\ \text{AQ@SiO}_2 \text{ (flow)} \end{matrix}} \text{Ar}^1\text{C}(\text{OZ})\text{H} + \text{HCOOH} + \text{Ar}^2\text{OX}$ $\text{Z} = \text{H or OH}$			
	Conversion	Yield	
2a	99% 97% 99%	96% 93% 98%	35% 29% 32%
2b	98% 99% 89%	47% 57% 36%	52% 42% 51%
2c	99% 88% 98%	78% 71% 73%	23% 28% 26%
2d	95% 94% 80%	87% 77% 76%	<i>n.d.</i> <i>n.d.</i> 2%
2e	98% 99% 94%	92% 89% 90%	<i>n.d.</i> 3% 5%
2f	99% ^a 99% ^a 98%	89% 90% 93%	59% 63% 55%

Figure 5. Scope of cleavage of lignin model dimers. ^aReaction time 40 h.

After achieving promising results with dimer cleavage, we proceeded to test our method on a polymeric model before applying it to real lignin samples.⁴¹ While the dimer studies demonstrated excellent outcomes, lignin's inherently complex polymeric structure posed additional challenges. To bridge this gap, we synthesized a polymeric model that closely mimics the structure of natural lignin and subjected it to our reaction conditions. This approach facilitated a more straightforward analysis of the degradation process, offering deeper insights into the catalyst's behavior. Heteronuclear Single Quantum Coherence (HSQC) analysis clearly confirmed the cleavage of β -O-4 bonds,

along with a shift in the aromatic region, indicating the formation of new species (Figure 6A). Additionally, gel permeation chromatography (GPC) analysis revealed that the synthetic polymer (G) initially had a molecular weight (Mw) of 3024 g/mol. After 16 hours of irradiation using our supported catalyst, the average molecular weight was significantly reduced to 623 g/mol, with peaks corresponding to dimers and monomers observed (Figure 6B).

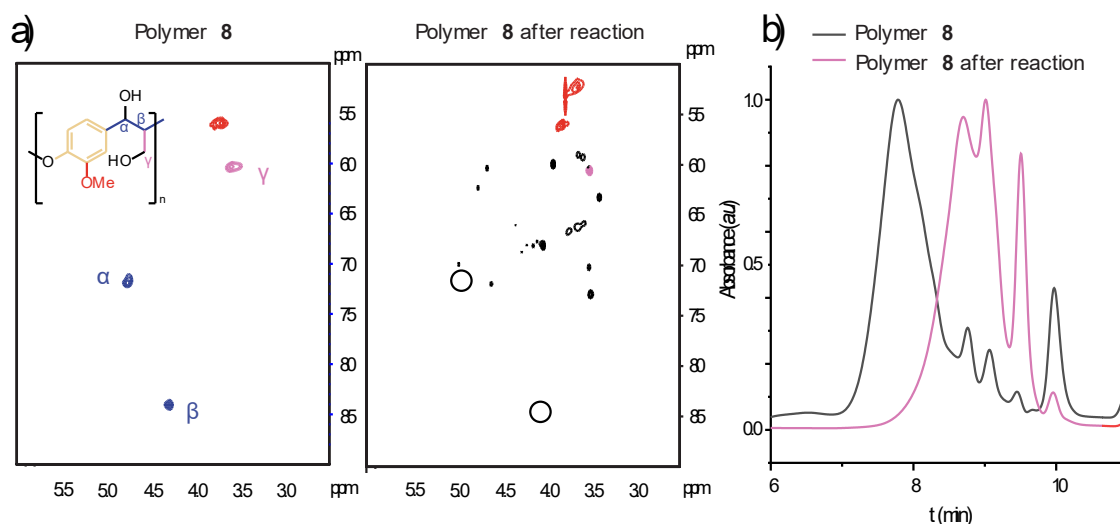


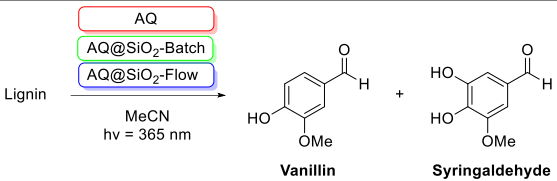
Figure 6. a) HSQC spectra and b) GPC chromatogram of polymer **8** before and after reaction with AQ@SiO₂.

Having successfully concluded the study of lignin dimeric and polymeric models, we shifted our focus to real organosolv lignin. To this end, we selected lignin samples from various sources, including bamboo, and pine, representing both hardwood and softwood types. Our objective was to extract monomers such as vanillin and syringaldehyde. As with the lignin dimeric models, the lignin samples were subjected to three catalytic processes: homogeneous anthraquinone (AQ), supported anthraquinone on silica (AQ@SiO₂) under batch conditions, and AQ@SiO₂ under flow conditions. Table 3 presents both the total content of vanillin and syringaldehyde determined *via* the standardized nitrobenzene oxidation method,⁴² and the yields of these monomers relative to their total content in the samples under specified conditions.

In general, moderate yields were obtained using homogeneous anthraquinone as catalyst, while the supported catalyst (AQ@SiO₂) typically improved the yields. Notably, the analysis of model compounds was performed in acetonitrile; however, real lignin samples often exhibited limited solubility in this solvent at high concentrations. To address this issue and minimize its impact on the reaction outcome, lignin samples were acetylated, resulting in significantly improved solubility in acetonitrile. This improvement is evident in the case of bamboo lignin (entry 2), where the acetylated

version showed significantly higher monomer yields compared to its unmodified counterpart (entry 1), yielding the corresponding acetylated monomers (vanillin acetate or syringaldehyde acetate). A similar trend was observed for pine lignin, which initially exhibited particularly low solubility, yielding only 15% of the total vanillin content with AQ@SiO₂. However, when considering only the soluble fraction, this corresponded to a 75% yield. The yield was further improved by performing the reaction with acetylated pine lignin (entry 4). Gram scale reaction was also performed with dioxasolv pine lignin under photochemical flow conditions. By doing so, vanillin was not only detected but also isolated in high purity in a 94% yield considering the soluble lignin fraction.

Table 3. Results of lignin depolymerization.

					
Entry	Lignin sample	Vanillin content (w/w%) ^a	Syringaldehyde content (w/w%) ^a	Vanillin Yield (%) ^b	Syringaldehyde yield (%) ^b
1	Bamboo	2.5	2.7	5%	8%
				28%	42%
				15%	19%
2	Acetylated Bamboo	2.4	2.6	12%	19%
				33%	34%
				85%	78%
3	Pine dioxasolv	7.4	traces	10 (47)%	-
				15 (75)%	-
				40 (94)%	-
4	Acetylated Pine dioxasolv	7.1	traces	15%	-
				29%	-
				17%	-

^a Total vanillin and syringaldehyde content determined according to literature *via* nitrobenzene alkaline oxidation, followed by GC-FID analysis after silylation with *N,O*-bis(trimethylsilyl)trifluoroacetamide. ^b Yield determined by GC-FID after silylation with *N,O*-bis(trimethylsilyl)trifluoroacetamide using ethylvanillin as internal standard.

Further characterization of the reaction extended beyond monomer analysis. The average molecular weight of the samples before and after the reaction was measured using GPC, and qualitative analysis was conducted *via* HSQC (Figures 7, S5 and table S1). As observed with the polymeric model, signals corresponding to β-O-4 linkages were notably weakened or depleted after the reaction (Figure 7A), accompanied by a significant reduction in the average molecular weight, as determined by GPC. To demonstrate scalability, a gram-scale reaction was performed using dioxasolv pine lignin under photochemical flow conditions. Vanillin was successfully detected and isolated in high purity, achieving a 94% yield based on the soluble lignin fraction (Figure 7C). proving the usefulness of the process.

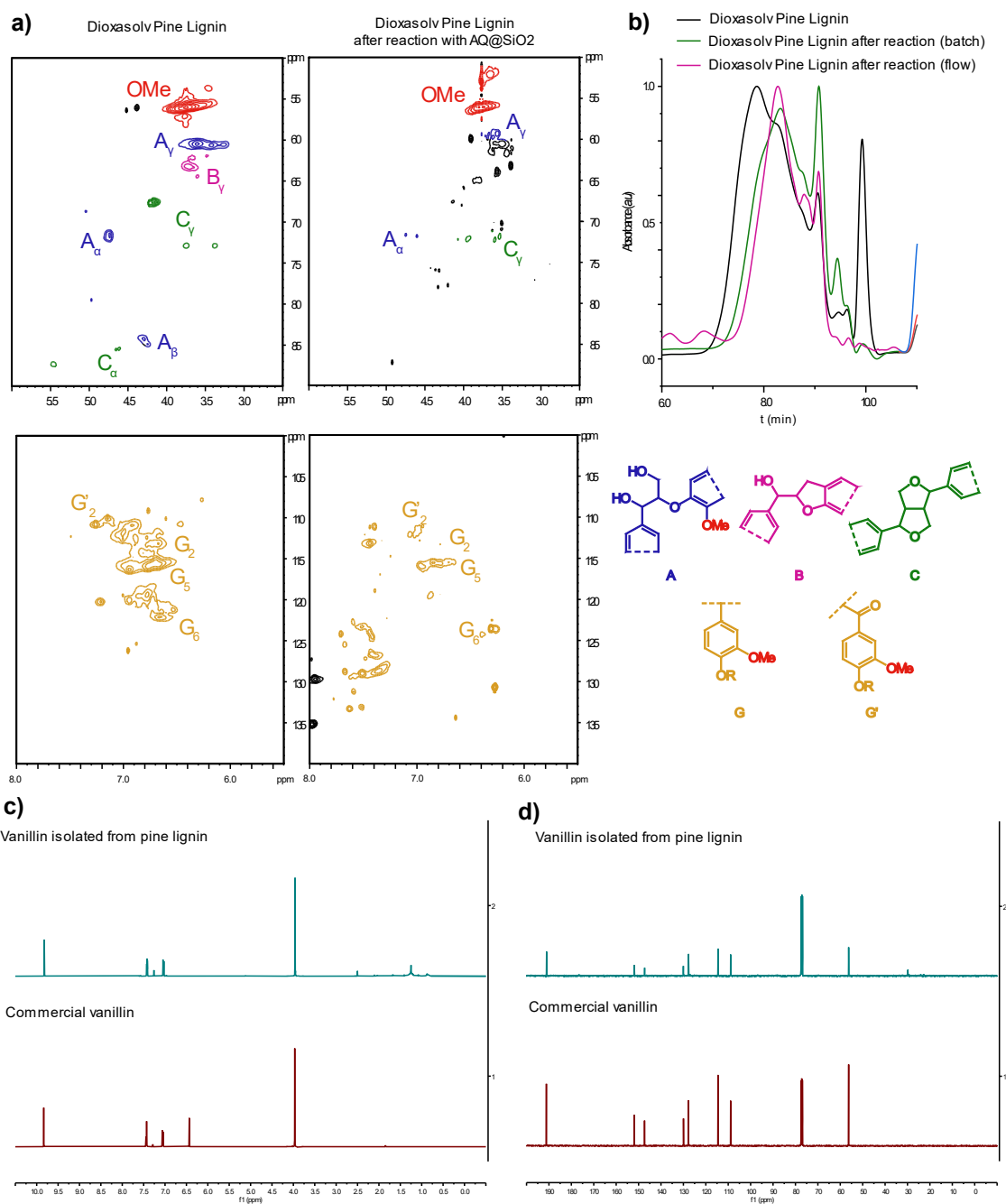


Figure 7. a) Selected examples of HSQC spectra of pine lignin before reaction and after reaction with AQ@SiO₂. b) GPC chromatographs of lignin before and after reaction. c) ¹H NMR and d) ¹³C NMR spectra of isolated vanillin after photochemical depolymerization of pine lignin and commercial vanillin.

As seen in figure 7 and table 3, we were able to obtain monomers such as vanillin, but a residue of oligomers was still present. Thus, we envisioned a way to valorize this residue in some application that prevents us from relying on fossil reserves. Apart from fuels, another field in which fossil resources are unmatched is in the polymers area. Nowadays, petrol-based polymers such as polystyrene are trying to be replaced by biorenewable and biodegradable materials, such as Poly(lactide) (PLA), which has gained great relevance in recent decades due to its environmentally friendly attributes, stemming from its biodegradability and its origin from renewable resources.⁴³ PLA exhibits interesting properties, such as high mechanical strength, transparency,

moderate barrier properties, and rather good processability, making it an ideal candidate for diverse applications in automotive industry, packaging, biomedical devices, tissue engineering, and 3D printing.^{44, 45, 46, 47, 48} However, its widespread use is hindered by critical limitations, related to its intrinsic brittleness, which restricts its use in applications requiring high impact resistance. To improve the mechanical properties of PLA and reduce its cost, formulation with different additives have been reported. In this sense, lignin has been proposed a promising filler for PLA composites offering the potential to achieve a balance of low cost, and multifunctionality, all while adhering to principles of biodegradability and sustainability. However, the poor compatibility between PLA and lignin significantly impacts the overall performance of these composites, posing a major challenge to their development.⁴⁹ One technical approach to overcome this drawback is plasticization⁵⁰. The addition of a plasticizer to PLA enhances the chain mobility as the free volume increases. This leads to a reduction in the glass transition temperature (T_g), serving as a quantifiable parameter to evaluate the plasticization efficiency.⁵¹ Various compounds, including monomeric plasticizers such as citrates⁵², carbonates⁵³, cinnamates⁵⁴, terpenes⁵⁵, adipates⁵⁶, as well as oligomeric/polymeric plasticizers such as lactic acid oligomers (OLA),⁵⁷ polyethylene glycol (PEG)⁵⁸, and others, have been extensively explored to improve the mechanical flexibility and toughness of PLA. An emerging alternative with significant potential involves the use waste materials as base compounds for designing new efficient plasticizers.^{59, 60, 61, 62, 63, 64} Thus, instead of using lignin as a mere filler, we envisioned its use as plastification agent. Oligomers resulting after our photochemical lignin valorization process were rich in phenolic compounds, and therefore they could be esterified with fatty acids. The unique molecular architecture of the resulting esters incorporates aromatic rings that enhance polarity, while ester groups provide interactions with aliphatic polyester chains, and hydrocarbon chains can contribute to flexibility.^{65, 66} This combination of features positions lignin-based esters as promising plasticizers to mitigate PLA's brittleness while maintaining its eco-friendly profile and providing it with enhanced toughness.

Lignin oligomers residue obtained after photochemical reaction of organosolv bamboo lignin were subjected to a esterification process with two naturally occurring carboxylic acids, namely caprylic and oleic acids. Unfragmented organosolv bamboo lignin was subjected to the same process for comparison purposes. The plasticized materials consisting of PLA were successfully processed by extrusion and injection molding processes. As expected, due to the intense dark brown color of all three lignin-based esters, plasticized samples with these esters showed a dark brown opaque appearance typical of lignin-containing blends^{67, 68} (see supporting information for further details). Some softwoods show color coordinates in this same region,⁶⁹ thus indicating these materials based on PLA and lignin-based esters show a wood-like appearance (Table S2, Figure S10).

As previously indicated, one of the main drawbacks of PLA is its intrinsic brittleness, with elongation at break values of 10-12%, and lower. Plasticizers can improve toughness by increasing the free volume and allowing chain mobility. This can be assessed by thermal analysis and, specifically, with differential scanning calorimetry (DSC) which allow observation of the main thermal transitions of PLA and its plasticized formulations (Figure 8A). At room temperature, PLA is stiff polymer characterized by glass transition temperature, T_g , of 55 – 60 °C.⁷⁰ Regarding esters of raw lignin with caprylic acid (PLA-xL-CA), they exert some plasticization on PLA as can be seen by a reduction in T_g to values of 51.7 °C, and 47.2 °C for 10 wt.%, and 20 wt.%, respectively (Table S3). The results obtained with the esters of waste lignin resulting from fragmentation (WL) are different, depending on the fatty acid used for esterification. WL esterified with oleic acid, shows a clear plasticization effect that can be assessed by a decrease of T_g to values comprised in the 49 – 52 °C, and a noticeable decrease in the peak maximum of the cold crystallization process to such low values of 84 – 88 °C, thus suggesting better plasticization efficiency than esters of raw lignin (L). Interestingly, esters of waste lignin with caprylic acid show a different behavior. At 10 wt.% (PLA-10WL-CA), the T_g is not decreased, but a slight increase can be seen. Nevertheless, at 20 wt.% (PLA-20WL-CA), the decrease in T_g is similar to that observed for the other lignin-based esters. Anyway, this decrease in T_g is comparable, or higher, to that observed with some commonly used modified vegetable oils as shown, with epoxidized palm oil (EPO)⁷¹ or maleinized linseed oil (MLO).⁷² By considering the theoretical enthalpy of a 100% crystalline PLA to be 93.6 J/g⁷³, the degree of crystallinity (χ_c) developed by all the materials after processing by extrusion and injection moulding,[—] and the maximum crystallinity these materials can reach, (χ_{c_max}), is also provided in Table S2). Plasticizers based on waste lignin fragmentation, lead to higher χ_c , and χ_{c_max} values. This phenomenon suggests the increased chain mobility provided by the plasticizers have a positive effect on both the χ_{c_max} ranging from 52 – 56%, as well as on χ_c with values of 32.6% for PLA-20WL-OA.

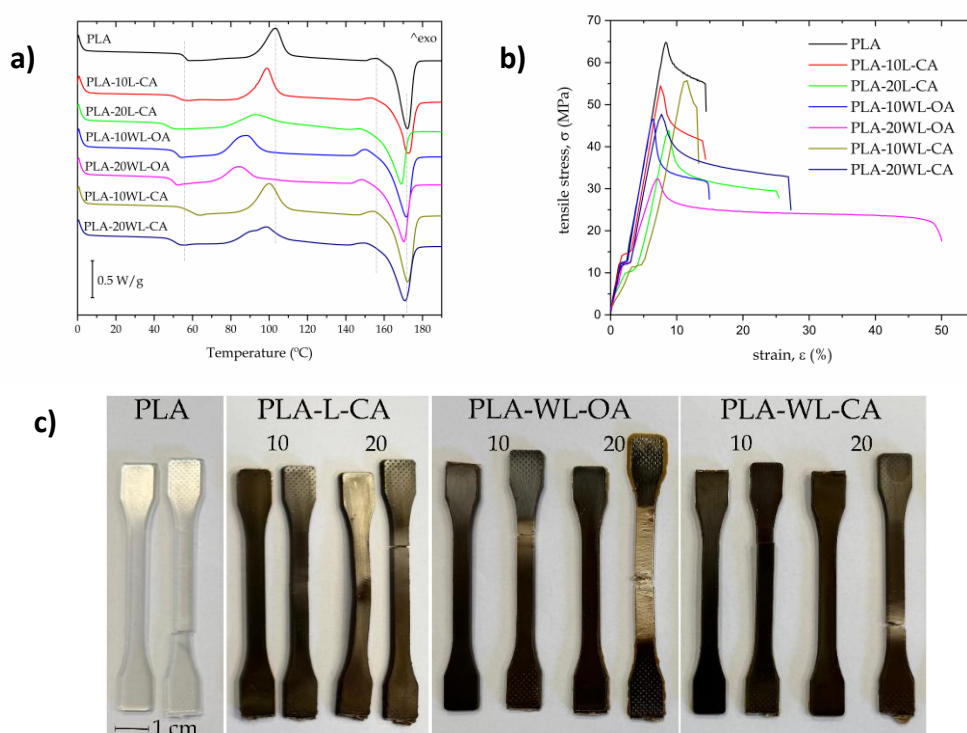


Figure 8. a) Comparative plot of the DSC (first heating) thermograms of PLA and PLA plasticized with lignin-based esters. b) Stress (σ)-strain (ϵ) curves obtained by tensile tests, and b) Visual appearance of the injection-molded specimens before and after the tensile test of PLA and PLA plasticized with lignin-based esters. c) Visual appearance of specimens before and after tensile test, corresponding to PLA and PLA plasticized with lignin-based esters.

The effect of plasticization is reflected in mechanical properties as seen in Table S3. As previously indicated, PLA is a rather brittle polymer with very low elongation at break (ϵ_b) of 14.4%, and a tensile strength (σ_{\max}) of 67.4 MPa. At low concentrations (10 wt.%) of the different lignin-based esters, the improvement in ductile properties is almost negligible. Nevertheless, DSC results have shown a decrease in T_g in almost all lignin-based esters thus confirming plasticization, which is in fact reflected in a clear decrease in maximum tensile strength at a concentration of 10 wt.% lignin-based esters and is much more pronounced for plasticized PLA formulations containing 20 wt.% lignin-based esters. Moreover, at 20 wt.% lignin-based esters, the plasticization effect is not only detectable by a decrease in σ_{\max} , but also by a noticeable increase in ϵ_b . Best results were obtained with PLA-20WL-OA, showing the highest elongation at break of 46.1% (Figure 8-b). Despite these values are far from some of the best plasticizers recently reported in this research area^{54, 74, 75}, it is worthy to note they are similar, or even higher to those reported in plasticized PLA with vegetable oil-derived plasticizers.^{76, 77, 78, 79}

The impact strength of neat PLA is 2.1 kJ/m². This increases up to values of 6.4 kJ/m², and 5.2 kJ/m² for PLA-20WL-OA, and PLA-20WL-CA, respectively, thus showing a noticeable increase in the ability of the plasticized formulations to absorb energy. The

increase in toughness has also been evaluated by calculating the work of fracture as the area under the stress (σ) – strain (ϵ) curves. Neat PLA shows a low value of 5.9 MJ/m³, consistent with literature reports,^{80, 81} and is increased up to 11.7 MJ/m³ for PLA-20WL-OA, thus showing the exceptional effect of these lignin-based esters on reducing PLA brittleness. These results suggest waste lignin fragmentation esters with oleic acid, show the best performance as biobased plasticizers for improved PLA toughness. Accordingly, PLA-20WL-OA is the only formulation showing a noticeable decrease in the Shore D with a value of 72.3 while all other materials in this work show a Shore D hardness of 80-83. Figure 8-c gathers the optical images of the tensile specimens before and after the uniaxial tensile test. As it can be seen, PLA is rather brittle, with very low elongation at break; nevertheless, plasticized PLA with waste lignin fragmentation esters with oleic acid (PLA-10WL-OA, and PLA-20WL-OA), show an increment in ductile properties with clear evidence of plastic deformation.

These materials also show an exceptional shape memory behavior. They can be deformed to a temporary shape at room temperature, due to the toughness these plasticizers provide to brittle PLA. After plastic deformation, the materials retain the deformed shape and when heated above their characteristic glass transition, they recover the initial shape as can be seen in Supplementary Information.

Conclusions.

A photochemical process for lignin valorization based on anthraquinone moiety has been successfully developed. The photocatalytic system is able to operate in batch and flow conditions thanks to an immobilization of the sensitizer on silica particles. Different samples of lignin derived from beech, pine and bamboo have been submitted to this protocol, yielding industrially relevant monomers, such as vanillin and a mixture of oligomer waste that has been employed as polylactic acid plasticizer after a simple esterification with fatty acids. Addition of 20 wt.% esters of waste lignin with oleic acids leads to a noticeable decrease in the glass transition temperature (T_g), which is reflected in improved ductility and toughness. Additionally, these materials show a withstanding shape memory behavior which can be very useful in self-repair PLA-based structures. Therefore, a holistic lignin valorization method has been developed, in which no lignin-derived residue is wasted.

Acknowledgements

N.G. thanks the support from grant “Ramon y Cajal” (RYC2018-023888-I) funded by MCIN/AEI/10.13039/501100011033. Likewise, N.G. wants to acknowledge the support received *via* the grants CNS2023-145354 and PID2021-128805NA-I00 funded by MCIN/AEI/10.13039/501100011033 and by the “European Union Next Generation EU/PRTR”. X.M. wants to acknowledge the support received *via* Spanish Ministerio de Ciencia e Innovación (PID2021-127332NB). This project has also received funding from the European Research Council (ERC) under the European Union’s Horizon 2020

research and innovation program (grant agreement No.948829). R.B. wants to acknowledge the support received *via* grant PID2023-152869OB-C22, and the grant TED2021-131762A-I00, funded by MCIN/AEI/10.13039/501100011033 and by the European Union “NextGenerationEU”/PRTR. The authors also thank Generalitat Valenciana - GVA, grant number CIGE/2023/46 and CIAICO/2023/253, for supporting this work. J.G.-C. wants to thank FPU20/01732 grant funded by MCIN/AEI/10.13039/501100011033 and by ESF Investing in your future.

Author contributions

X.M. and N.G. wrote and revised the manuscript. X.M. performed the chemical experiment and data analyses, S.M.-V. and E.R. prepared lignin samples and set up the analysis equipment. U.A. performed the DFT calculations. J.G.-C., M.M.-P. and R.B. performed the PLA plasticization experiments and material characterization. All authors reviewed and approved the final manuscript.

Competing interests. The authors declare no competing interests.

Supplementary information The online version contains supplementary material.

Correspondence and requests for materials should be addressed to N.G.: nestor.guijarro@ua.es.

References

1. Brockway PE, Owen A, Brand-Correa LI, Hardt L. Estimation of global final-stage energy-return-on-investment for fossil fuels with comparison to renewable energy sources. *Nat Energy* **4**, 612-621 (2019).
2. McGlade C, Ekins P. The geographical distribution of fossil fuels unused when limiting global warming to 2 °C. *Nature* **517**, 187-190 (2015).
3. Pellegrini L, Arsel M, Muñoa G, Rius-Taberner G, Mena C, Orta-Martínez M. The atlas of unburnable oil for supply-side climate policies. *Nat Commun* **15**, 2318 (2024).
4. Jiang M, *et al.* Tracing fossil-based plastics, chemicals and fertilizers production in China. *Nat Commun* **15**, 3854 (2024).
5. Zhang B, Biswal BK, Zhang J, Balasubramanian R. Hydrothermal Treatment of Biomass Feedstocks for Sustainable Production of Chemicals, Fuels, and Materials: Progress and Perspectives. *Chem Rev* **123**, 7193-7294 (2023).
6. Lopez G, Keiner D, Fasihi M, Koironen T, Breyer C. From fossil to green chemicals: sustainable pathways and new carbon feedstocks for the global chemical industry. *Energy Environ Sci* **16**, 2879-2909 (2023).

7. Segers B, *et al.* Lignocellulosic biomass valorisation: a review of feedstocks, processes and potential value chains and their implications for the decision-making process. *RSC Sustain* **2**, 3730-3749 (2024).
8. Larsen J, Haven MØ, Thirup L. Inbicon makes lignocellulosic ethanol a commercial reality. *Biomass Bioenergy* **46**, 36-45 (2012).
9. Klemm D, Heublein B, Fink H-P, Bohn A. Cellulose: Fascinating Biopolymer and Sustainable Raw Material. *Angew Chem Int Ed* **44**, 3358-3393 (2005).
10. Rao J, Lv Z, Chen G, Peng F. Hemicellulose: Structure, chemical modification, and application. *Prog Polym Sci* **140**, 101675 (2023).
11. Sivagurunathan P, *et al.* 2G waste lignin to fuel and high value-added chemicals: Approaches, challenges and future outlook for sustainable development. *Chemosphere* **268**, 129326 (2021).
12. Eswaran Scd, Subramaniam S, Sanyal U, Rallo R, Zhang X. Molecular structural dataset of lignin macromolecule elucidating experimental structural compositions. *Sci Data* **9**, 647 (2022).
13. Zakzeski J, Bruijninx PCA, Jongerius AL, Weckhuysen BM. The Catalytic Valorization of Lignin for the Production of Renewable Chemicals. *Chem Rev* **110**, 3552-3599 (2010).
14. Li C, Zhao X, Wang A, Huber GW, Zhang T. Catalytic Transformation of Lignin for the Production of Chemicals and Fuels. *Chem Rev* **115**, 11559-11624 (2015).
15. Leng E, Guo Y, Chen J, Liu S, E J, Xue Y. A comprehensive review on lignin pyrolysis: Mechanism, modeling and the effects of inherent metals in biomass. *Fuel* **309**, 122102 (2022).
16. Tillou JG, Ezeorah CJ, Kuchta JJ, Dissanayake Mudiyanse SCD, Sitter JD, Vannucci AK. A review on recent trends in selective hydrodeoxygenation of lignin derived molecules. *RSC Sustain* **1**, 1608-1633 (2023).
17. Nandiwale KY, *et al.* Enhanced Acid-Catalyzed Lignin Depolymerization in a Continuous Reactor with Stable Activity. *ACS Sustain Chem Eng* **8**, 4096-4106 (2020).
18. F. De Gregorio G, *et al.* Oxidative Depolymerization of Lignin Using a Novel Polyoxometalate-Protic Ionic Liquid System. *ACS Sustain Chem Eng* **4**, 6031-6036 (2016).
19. Gazi S, Hung Ng WK, Ganguly R, Putra Moeljadi AM, Hirao H, Soo HS. Selective photocatalytic C–C bond cleavage under ambient conditions with earth abundant vanadium complexes. *Chem Sci* **6**, 7130-7142 (2015).

20. Wang H, Giardino GJ, Chen R, Yang C, Niu J, Wang D. Photocatalytic Depolymerization of Native Lignin toward Chemically Recyclable Polymer Networks. *ACS Cent Sci* **9**, 48-55 (2023).
21. Bosque I, Magallanes G, Rigoulet M, Kärkäs MD, Stephenson CRJ. Redox Catalysis Facilitates Lignin Depolymerization. *ACS Cent Sci* **3**, 621-628 (2017).
22. Cervantes-González J, *et al.* Anthraquinones: Versatile Organic Photocatalysts. *ChemCatChem* **12**, 3811-3827 (2020).
23. Chen C-X, *et al.* Anthraquinones-based photocatalysis: A comprehensive review. *Environ Sci Ecotechnology* **22**, 100449 (2024).
24. Zhou Y, Hu D, Li D, Jiang X. Uranyl-Photocatalyzed Hydrolysis of Diaryl Ethers at Ambient Environment for the Directional Degradation of 4-O-5 Lignin. *JACS Au* **1**, 1141-1146 (2021).
25. Cismesia MA, Yoon TP. Characterizing chain processes in visible light photoredox catalysis. *Chem Sci* **6**, 5426-5434 (2015).
26. Zhong P-F, *et al.* Photoelectrochemical oxidative C(sp³)-H borylation of unactivated hydrocarbons. *Nat Commun* **14**, 6530 (2023).
27. Wu K, Cao M, Zeng Q, Li X. Radical and (photo)electron transfer induced mechanisms for lignin photo- and electro-catalytic depolymerization. *Green Energy Environ* **8**, 383-405 (2023).
28. Wang Y, Liu Y, He J, Zhang Y. Redox-neutral photocatalytic strategy for selective C-C bond cleavage of lignin and lignin models via PCET process. *Sci Bull* **64**, 1658-1666 (2019).
29. Aprà E, *et al.* NWChem: Past, present, and future. *The Journal of Chemical Physics* **152**, (2020).
30. Becke AD. Density-functional thermochemistry. III. The role of exact exchange. *The Journal of Chemical Physics* **98**, 5648-5652 (1993).
31. Ditchfield R, Hehre WJ, Pople JA. Self-Consistent Molecular-Orbital Methods. IX. An Extended Gaussian-Type Basis for Molecular-Orbital Studies of Organic Molecules. *The Journal of Chemical Physics* **54**, 724-728 (1971).
32. Hehre WJ, Ditchfield R, Pople JA. Self-Consistent Molecular Orbital Methods. XII. Further Extensions of Gaussian-Type Basis Sets for Use in Molecular Orbital Studies of Organic Molecules. *The Journal of Chemical Physics* **56**, 2257-2261 (1972).

33. Hariharan PC, Pople JA. The influence of polarization functions on molecular orbital hydrogenation energies. *Theoretica chimica acta* **28**, 213-222 (1973).
34. Valduga AT, Gonçalves IL, Saorin Puton BM, de Lima Hennig B, Sousa de Brito E. Anthraquinone as emerging contaminant: technological, toxicological, regulatory and analytical aspects. *Toxicol Res* **40**, 11-21 (2024).
35. Guadalupe Martin M, Lázaro-Martínez JM, Martín SE, Uberman PM, Budén ME. Anthraquinone-Modified Silica Nanoparticles as Heterogeneous Photocatalyst for the Oxidative Hydroxylation of Arylboronic Acids. *Chem Eur J* **30**, e202303382 (2024).
36. Liu R, Cheng S-C, Xiao Y, Chan K-C, Tong K-M, Ko C-C. Recyclable polymer-supported iridium-based photocatalysts for photoredox organic transformations. *J Catal* **407**, 206-212 (2022).
37. Do PQT, *et al.* The highly sensitive determination of serotonin by using gold nanoparticles (Au NPs) with a localized surface plasmon resonance (LSPR) absorption wavelength in the visible region. *RSC Adv* **10**, 30858-30869 (2020).
38. Maglione MS, *et al.* Fluid Mixing for Low-Power 'Digital Microfluidics' Using Electroactive Molecular Monolayers. *Small* **14**, 1703344 (2018).
39. Lindroth R, Materna KL, Hammarström L, Wallentin C-J. Sustainable Ir-Photoredox Catalysis by Means of Heterogenization. *ACS Org Inorg Au* **2**, 427-432 (2022).
40. Sambiagio C, Noël T. Flow Photochemistry: Shine Some Light on Those Tubes! *Trends Chem* **2**, 92-106 (2020).
41. Talebi Amiri M, Bertella S, Questell-Santiago YM, Luterbacher JS. Establishing lignin structure-upgradeability relationships using quantitative ¹H–¹³C heteronuclear single quantum coherence nuclear magnetic resonance (HSQC-NMR) spectroscopy. *Chem Sci* **10**, 8135-8142 (2019).
42. Dong L, *et al.* Breaking the Limit of Lignin Monomer Production via Cleavage of Interunit Carbon–Carbon Linkages. *Chem* **5**, 1521-1536 (2019).
43. Shekhar N, Mondal A. Synthesis, properties, environmental degradation, processing, and applications of Polylactic Acid (PLA): an overview. *Polym Bull* **81**, 11421-11457 (2024).
44. Costabeber G, *et al.* Additive manufacturing of polylactic acid scaffolds dip-coated with polycaprolactone for bone tissue engineering. *Mater Today Commun* **40**, (2024).

45. Abedsoltan H. Applications of plastics in the automotive industry: Current trends and future perspectives. *Polym Eng Sci* **64**, 929-950 (2024).
46. Khouri NG, Bahú JO, Blanco-Llamero C, Severino P, Concha VOC, Souto EB. Polylactic acid (PLA): Properties, synthesis, and biomedical applications - A review of the literature. *J Mol Struct* **1309**, 138243 (2024).
47. Rajendran DS, Venkataraman S, Jha SK, Chakrabarty D, Kumar VV. A review on bio-based polymer polylactic acid potential on sustainable food packaging. *Food Sci Biotechnol* **33**, 1759-1788 (2024).
48. Arockiam AJ, Subramanian K, Padmanabhan RG, Selvaraj R, Bagal DK, Rajesh S. A review on PLA with different fillers used as a filament in 3D printing. In: *2nd International Conference on Functional Material, Manufacturing and Performances (ICFMMP)* (ed[^](eds). SI edn (2021).
49. Ye H, You T, Nawaz H, Xu F. A comprehensive review on polylactic acid/lignin composites — Structure, synthesis, performance, compatibilization, and applications. *Int J Biol Macromol* **280**, 135886 (2024).
50. Mazidi MM, Arezoumand S, Zare L. Research progress in fully biorenewable tough blends of polylactide and green plasticizers. *Int J Biol Macromol* **279**, 135345 (2024).
51. Llanes LC, Clasen SH, Pires ATN, Gross IP. Mechanical and thermal properties of poly(lactic acid) plasticized with dibutyl maleate and fumarate isomers: Promising alternatives as biodegradable plasticizers. *Eur Polym J* **142**, 110112 (2021).
52. Hassouna F, Raquez JM, Addiego F, Toniazzo V, Dubois P, Ruch D. New development on plasticized poly(lactide): Chemical grafting of citrate on PLA by reactive extrusion. *Eur Polym J* **48**, 404-415 (2012).
53. Seo HJ, *et al.* Glycerol-derived organic carbonates: environmentally friendly plasticizers for PLA. *RSC Adv* **14**, 4702-4716 (2024).
54. Barandiaran A, *et al.* Esters of Cinnamic Acid as Green Plasticizers for Polylactide Formulations with Improved Ductility. *Macromol Mater Eng* **308**, 2300022 (2023).
55. Tejada-Oliveros R, Gomez-Caturla J, Fenollar O, Montanes N, Ivorra-Martinez J, Garcia-Garcia D. Assessment of non-ester monoterpenoids as biobased plasticizers for polylactide with improved ductile behaviour. *Polymer* **290**, 126572 (2024).

56. Shirai MA, Grossmann MVE, Mali S, Yamashita F, Garcia PS, Müller CMO. Development of biodegradable flexible films of starch and poly(lactic acid) plasticized with adipate or citrate esters. *Carbohydr Polym* **92**, 19-22 (2013).
57. Litauszki K, Pettrény R, Haramania Z, Mészáros L. Combined effects of plasticizers and D-lactide content on the mechanical and morphological behavior of polylactic acid. *Heliyon* **9**, e14674 (2023).
58. Shin H, Thanakkasaranee S, Sadeghi K, Seo J. Preparation and characterization of ductile PLA/PEG blend films for eco-friendly flexible packaging application. *Food Packag Shelf Life* **34**, (2022).
59. Tan JH, *et al.* Biodegradable Waste Frying Oil-Based Ethoxylated Esters as Highly Efficient Plasticizers for Poly(lactic acid). *ACS Sustain Chem Eng* **7**, 15957-15965 (2019).
60. Gartili A, Lapinte V, Caillol S, Briou B, Jego L. CNSL-based plasticizers, a promising and sustainable alternative to phthalates, a review. *RSC Sustain*, (2024).
61. Bäckströrn E, Odelius K, Hakkarainen M. Designed from Recycled: Turning Polyethylene Waste to Covalently Attached Polylactide Plasticizers. *ACS Sustain Chem Eng* **7**, 11004-11013 (2019).
62. Azwar E, Yin B, Hakkarainen M. Liquefied biomass derived plasticizer for polylactide. *J Chem Technol Biotechnol* **88**, 897-903 (2013).
63. Najera-Losada L, Narvaez-Rincón PC, Orjuela A, Gomez-Caturla J, Fenollar O, Balart R. Plasticization of Polylactide Using Biobased Epoxidized Isobutyl Esters Derived from Waste Soybean Oil Deodorizer Distillate. *J Environ Polym Degrad*, (2024).
64. D'Amico DA, *et al.* Repurpose of used frying sunflower oil as an ecofriendly plasticizer for polylactic acid. *Ind Crops Prod* **214**, 118467 (2024).
65. Yang Y, Huang JC, Zhang RY, Zhu J. Designing bio-based plasticizers: Effect of alkyl chain length on plasticization properties of isosorbide diesters in PVC blends. *Mater Des* **126**, 29-36 (2017).
66. Bocque M, Voirin C, Lapinte V, Caillol S, Robin JJ. Petro-Based and Bio-Based Plasticizers: Chemical Structures to Plasticizing Properties. *J Polym Sci, Part A: Polym Chem* **54**, 11-33 (2016).
67. Montes MLI, *et al.* Design and Characterization of PLA Bilayer Films Containing Lignin and Cellulose Nanostructures in Combination With Umbelliferone as Active Ingredient. *Front Chem* **7**, (2019).

68. Ajao O, Jaaidi J, Benali M, Restrepo AM, El Mehdi N, Boumghar Y. Quantification and Variability Analysis of Lignin Optical Properties for Colour-Dependent Industrial Applications. *Molecules* **23**, 377 (2018).
69. de Almeida TH, de Almeida DH, Gonsalves D, Lahr FAR. Color variations in CIELAB coordinates for softwoods and hardwoods under the influence of artificial and natural weathering. *J Build Eng* **35**, 101965 (2021).
70. Blázquez-Blázquez E, Barranco-García R, Díez-Rodríguez TM, Cerrada ML, Pérez E. Role of the plasticizers on the crystallization of PLA and its composites with mesoporous MCM-41. *J Mater Sci* **59**, 6305-6321 (2024).
71. Chieng BW, Ibrahim NA, Then YY, Loo YY. Epoxidized Vegetable Oils Plasticized Poly(lactic acid) Biocomposites: Mechanical, Thermal and Morphology Properties. *Molecules* **19**, 16024-16038 (2014).
72. Ferri JM, Garcia-Garcia D, Montanes N, Fenollar O, Balart R. The effect of maleinized linseed oil as biobased plasticizer in poly (lactic acid)-based formulations. *Polym Int* **66**, 882-891 (2017).
73. Song LX, *et al.* Crystallization, Structure and Significantly Improved Mechanical Properties of PLA/PPC Blends Compatibilized with PLA-PPC Copolymers Produced by Reactions Initiated with TBT or TDI. *Polymers* **13**, 3245 (2021).
74. Gomez-Caturla J, *et al.* Improvement of Poly(lactide) Ductile Properties by Plasticization with Biobased Tartaric Acid Ester. *Macromol Mater Eng* **308**, 2200694 (2023).
75. Gomez-Caturla J, Ivorra-Martinez J, Tejada-Oliveros R, Moreno, Garcia-Garcia D, Balart R. Effect of the chain length of geraniol esters on the plasticization efficiency with poly(lactide). *Polymer* **290**, 126522 (2024).
76. Garcia-Garcia D, Carbonell-Verdu A, Arrieta MP, López-Martínez J, Samper MD. Improvement of PLA film ductility by plasticization with epoxidized karanja oil. *Polym Degrad Stab* **179**, 109259 (2020).
77. Ruellan A, *et al.* Industrial vegetable oil by-products increase the ductility of polylactide. *EXPRESS Polym Lett* **9**, 1087-1103 (2015).
78. Sen I, Atagür M, Tuna S, Eroglu M, Kurtlu MA, Sever K. Manufacturing and Characterization of Three Modified Vegetable Oil-Added Polylactic Acid Composites. *Int J Polym Sci* **2024**, 3259882 (2024).
79. Carbonell-Verdu A, Garcia-Garcia D, Dominici F, Torre L, Sanchez-Nacher L, Balart R. PLA films with improved flexibility properties by using maleinized cottonseed oil. *Eur Polym J* **91**, 248-259 (2017).

80. Zhang CM, Huang Y, Luo CH, Jiang L, Dan Y. Enhanced ductility of polylactide materials: Reactive blending with pre-hot sheared natural rubber. *J Polym Res* **20**, 121 (2013).
81. Ramlee NA, Tominaga Y. Mechanical and degradation properties in alkaline solution of poly(ethylene carbonate)/poly(lactic acid) blends. *Polymer* **166**, 44-49 (2019).